

# Estimation of anisotropic bending rigidities and spontaneous curvatures of crescent curvature-inducing proteins from tethered-vesicle experimental data

Hiroshi Noguchi,<sup>1,\*</sup> Nikhil Walani,<sup>2,3</sup> and Marino Arroyo<sup>2,4,5</sup>

<sup>1</sup>*Institute for Solid State Physics, University of Tokyo, Kashiwa, Chiba 277-8581, Japan*

<sup>2</sup>*Universitat Politècnica de Catalunya-BarcelonaTech, 08034 Barcelona, Spain*

<sup>3</sup>*Present address: Department of Applied Mechanics, IIT Delhi, Hauz Khas, New Delhi, 110016, India*

<sup>4</sup>*Institute for Bioengineering of Catalonia (IBEC),*

*The Barcelona Institute for Science and Technology (BIST), 08028 Barcelona, Spain*

<sup>5</sup>*Centre Internacional de Mètodes Numèrics en Enginyeria (CIMNE), 08034 Barcelona, Spain*

The Bin/amphiphysin/Rvs (BAR) superfamily proteins have a crescent binding domain and bend biomembranes along the domain axis. However, their anisotropic bending rigidities and spontaneous curvatures have not been experimentally determined. Here, we estimated these values from the bound protein densities on tethered vesicles using a mean-field theory of anisotropic bending energy and orientation-dependent excluded volume. The dependence curves of the protein density on the membrane curvature are fitted to the experimental data for the I-BAR and N-BAR domains reported by C. Prévost et al. *Nat. Commun.* **6**, 8529 (2015) and F.-C. Tsai et al. *Soft Matter* **17**, 4254 (2021), respectively. For the I-BAR domain, all three density curves of different chemical potentials exhibit excellent fits with a single parameter set of anisotropic bending energy. When the classical isotropic bending energy is used instead, one of the curves can be fitted well, but the others exhibit large deviations. In contrast, for the N-BAR domain, two curves are not well-fitted simultaneously using the anisotropic model, although it is significantly improved compared to the isotropic model. This deviation likely suggests a cluster formation of the N-BAR domains.

## I. INTRODUCTION

In living cells, membrane morphology is regulated by the binding and unbinding of curvature-inducing proteins [1–8]. Some types of these proteins bend a membrane in a laterally isotropic manner and generate spherical membrane buds [3–6]. In contrast, the Bin/amphiphysin/Rvs (BAR) superfamily proteins have a crescent binding domain (BAR domain) and bend membranes along the BAR domain axis, generating cylindrical membrane tubes [1–3, 9–12]. Several types of BAR domains are known: N-BARs and F-BARs bend membranes positively, but I-BARs bend them in the opposite direction.

These curvature-inducing proteins can sense membrane curvature; that is, their binding onto membranes depends on the local membrane curvatures. Tethered vesicles have been widely used to observe the curvature sensing experimentally [7, 8, 13–21]. A vesicle is pulled by optical tweezers and a micropipette to form a narrow membrane tube (tether). The tube radius can be controlled by adjusting the position of the optical tweezers. The curvature sensing of BAR proteins [7, 8, 13–15], G-protein coupled receptors (GPCRs) [16], ion channels [17, 18], dynamin [19], annexins [20], and Ras proteins [21] have been reported. Additionally, the curvature sensing has been detected by the protein binding onto different sizes of spherical vesicles [21–23].

Evaluating the mechanical properties of these proteins is crucial for quantitatively understanding their curva-

ture generation and sensing. The aim of this study is to determine the anisotropic bending rigidity and spontaneous curvature of BAR proteins from experimental data of tethered vesicles. In previous studies [13–15], the bending rigidity and spontaneous curvature of BAR proteins have been estimated using the Canham–Helfrich theory [24, 25]. However, this theory is formulated for laterally isotropic fluid membranes; thus, the anisotropy of the proteins is not considered. Recently, we developed a mean-field model for anisotropic bending energy and entropic interactions [26–28]. Orientational fluctuations are included based on Nascimentos’ theory for three-dimensional liquid crystals [29]. The first- and second-order transitions between isotropic and nematic phases are obtained with increasing protein density in narrow membrane tubes [28]. In the present study, we use this theoretical model to estimate the anisotropic bending rigidity and spontaneous curvature. The experimental data for the I-BAR domain of IRSp53 and the N-BAR domain of amphiphysin 1 reported in Refs. 14 and 15, respectively, are used for the estimation. In theoretical studies, a protein is often assumed to be a rigid body [30–33]. The membrane-mediated interaction of two rigid proteins qualitatively reproduces that of two flexible proteins obtained by meshless membrane simulations, but the amplitude is overestimated [34]. Hence, the estimation of the bending rigidity is also important for evaluating the interaction between proteins.

The mean-field theory and fitting method are described in Sec. II. Secs. III and IV present and discuss the fitting results for the I-BAR and N-BAR domains, respectively. Additionally, the results of the isotropic and anisotropic protein models are compared. Sec. V concludes the pa-

\* noguchi@issp.u-tokyo.ac.jp

per.

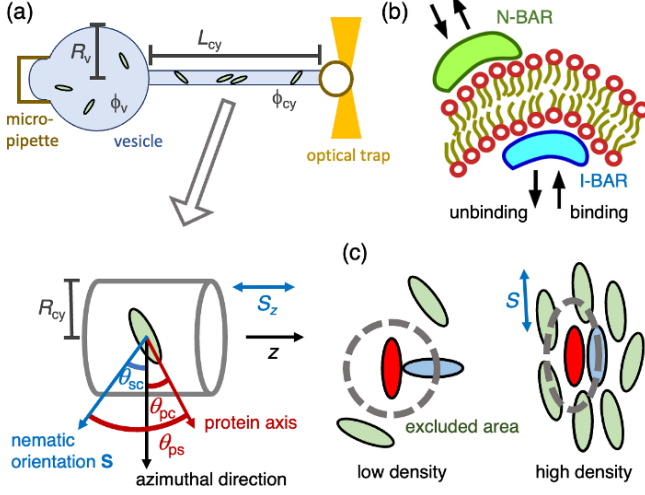


FIG. 1. Schematic of a tethered vesicle and protein binding. (a) Experimental setup of the tethered vesicle. The proteins are bound in the tether and spherical vesicle regions with bound densities of  $\phi_{cy}$  and  $\phi_v$ , respectively. The angles between the nematic direction  $\mathbf{S}$ , the azimuthal direction, and/or the protein axis are shown in the bottom panel. (b) Binding and unbinding of BAR domains. N-BAR and I-BAR domains bind onto the outer and inner surfaces of the vesicle, respectively. (c) Excluded-volume interactions between proteins. A perpendicular protein pair has a larger excluded area on the membrane surface (represented by thick dashed lines) than a parallel pair (compare the left and right panels).

## II. THEORY

A cylindrical membrane tube (tether) protrudes from the spherical vesicle, as depicted in Fig. 1(a). The tether length  $L_{cy}$  and radius  $R_{cy}$  are controlled by force  $f_{ex}$  generated by optical tweezers and a micropipette. The membrane is in a fluid phase and is homogeneous. The radius  $R_v$  of the spherical region is on a  $\mu\text{m}$  scale; thus, the membrane can be approximated as flat. The subscripts v and cy represent the quantities in the spherical and tether regions, respectively. The total membrane area  $A$  is fixed and the membrane area inside of the micropipette is assumed to be constant. The tether area  $A_{cy} = 2\pi R_{cy}L_{cy}$  is approximated as a constant, since the tube volume is negligibly small [35, 36]. The protein density  $\phi$  is the local area fraction covered by the bound proteins ( $\phi_v$  and  $\phi_{cy}$  represent the densities in the spherical and tether regions, respectively). N-BAR and I-BAR proteins bind onto the outer and inner surfaces, respectively (see Fig. 1(b)). Here, the curvature direction is defined as outward following the membrane curvature. Hence, the proteins binding to the inner surface have the opposite sign of curvature from the protein viewpoint (see I-BAR in Fig. 1(b)).

### A. Isotropic proteins

First, we describe the mean-field theory of proteins that bend membranes isotropically (no preferred lateral direction). The bending energy is given as follows: [37, 38]

$$F_{cv} = 4\pi\bar{\kappa}_d(1 - g_{ves}) + \int dA \left\{ 2\kappa_d H^2(1 - \phi) + \frac{\kappa_{pi}}{2}(2H - C_0)^2\phi + (\bar{\kappa}_{pi} - \bar{\kappa}_d)K\phi \right\}, \quad (1)$$

where  $g_{ves}$  represents the genus of the vesicle ( $g_{ves} = 0$  for tethered vesicles).  $H = (C_1 + C_2)/2$  and  $K = C_1C_2$  represent the mean and Gaussian curvatures of each position, respectively, with  $C_1$  and  $C_2$  being the principal curvatures. The bare (protein-unbound) membrane has a bending rigidity of  $\kappa_d$ , zero spontaneous curvature, and saddle-splay modulus of  $\bar{\kappa}_d$  (also called the Gaussian modulus) in the Canham-Helfrich theory [24, 25, 39]. The bound membrane has a bending rigidity of  $\kappa_{pi}$ , finite spontaneous curvature  $C_0$ , and saddle-splay modulus of  $\bar{\kappa}_{pi}$ . The first term of eqn (1) represents the integral over the Gaussian curvature  $K$ . Note that the curvature mismatch model [8, 14–16] and spontaneous curvature model [8, 15, 40, 41] are subsets of the present model for  $\kappa_{pi} > \kappa_d$  and  $\kappa_{pi} = \kappa_d$ , respectively [37]. For  $\kappa_{pi} < \kappa_d$ , the proteins exhibit curvature sensing but do not have a non-passive curvature-generation capability [38].

The membrane free energy  $F$  consists of the binding energy and mixing entropy in addition to the bending energy  $F_{cv}$ ,

$$F = F_{cv} + \int dA \left\{ -\frac{\mu}{a_p}\phi + \frac{k_B T}{a_p}[\phi \ln(\phi) + (1 - \phi) \ln(1 - \phi)] \right\}, \quad (2)$$

where  $a_p$  represents the area covered by one protein and  $k_B T$  represents the thermal energy. The maximum number of bound proteins is  $A/a_p$ . The first and second terms in the integral of eqn (2) represent the protein-binding energy with the chemical potential  $\mu$  and the mixing entropy of bound proteins, respectively. Here, we neglect the inter-protein interaction energy ( $\sim \phi^2$ ) [36–38], since we consider low protein densities in this study.

In thermal equilibrium, the protein density  $\phi$  is locally determined for each membrane curvature: [37, 38]

$$\phi = \frac{1}{1 + \exp(w_b)}, \quad (3)$$

$$w_b = -\frac{\mu}{k_B T} + \frac{a_p}{k_B T} \left( 2\kappa_{dif} H^2 + \bar{\kappa}_{dif} K - 2\kappa_{pi} C_0 H + \frac{\kappa_{pi} C_0^2}{2} \right), \quad (4)$$

where  $\kappa_{dif} = \kappa_{pi} - \kappa_d$  and  $\bar{\kappa}_{dif} = \bar{\kappa}_{pi} - \bar{\kappa}_d$ . Since the curvature of the spherical region of the tethered vesicles is approximated as  $H = K = 0$ , the protein density in the spherical region is given as  $\phi_v = 1/\{1 + \exp[(-\mu + a_p \kappa_{pi} C_0^2/2)/k_B T]\}$ . Hence, the protein density  $\phi_{cy}$  in the

tether regions is given as

$$\phi_{cy} = \frac{1}{1 + \frac{1-\phi_v}{\phi_v} \exp \left[ \frac{a_p}{k_B T} \left( \frac{\kappa_{dif}}{2R_{cy}^2} - \frac{\kappa_{pi}C_0}{R_{cy}} \right) \right]}. \quad (5)$$

When the membrane has the sensing curvature  $C_s$ ,  $\phi_{cy}$  is maximized. The sensing curvature is obtained from  $\phi_{cy}/(1/R_{cy}) = 0$ :

$$C_s = \frac{\kappa_{pi}C_0}{\kappa_{dif}}. \quad (6)$$

For  $\kappa_{dif} \neq 0$ , the numerator of the second term in parentheses can be replaced with  $\kappa_{dif}C_s$ , so that  $\kappa_{dif}$  and  $C_s$  can be used as fitting parameters. Here, the protein densities of tethered vesicles are independent of  $\kappa_{dif}$ , since  $R_v \gg R_{cy}$ . Note that at  $R_v \sim R_{cy}$ ,  $\phi_v$  is also dependent on  $\kappa_{dif}$  [38]. Thus, the density difference between small vesicles and tethers of the same mean curvature reported in Ref. 21 may be caused by this Gaussian curvature dependence. Other isotropic proteins, such as GPCRs [16] and ion channels [17, 18], may also have similar dependences.

For the low-density limit ( $\phi_{cy} \ll 1$ ), the density ratio is expressed by the exponential function [14, 36]

$$\frac{\phi_{cy}}{\phi_v} = \exp \left[ -\frac{a_p}{k_B T} \left( \frac{\kappa_{dif}}{2R_{cy}^2} - \frac{\kappa_{pi}C_0}{R_{cy}} \right) \right]. \quad (7)$$

The ratio  $\phi_{cy}/\phi_v$  is independent of  $\phi_v$  in this limit. Details regarding isotropic-protein binding on tethered vesicles are described in Ref. 36.

## B. Anisotropic proteins

Anisotropies of the protein bending energy and excluded volume are considered. The lateral shape of a bound protein is approximated as an ellipse with major and minor axis lengths of  $\ell_1$  and  $\ell_2$ , respectively. The aspect ratio is  $d_{el} = \ell_1/\ell_2$ , and the area is  $a_p = \pi\ell_1\ell_2/4$ . These proteins have an orientation-dependent excluded-volume interaction and can align on the membrane surface. When neighboring proteins have a perpendicularly orientation, the excluded area  $A_{exc}$  between them is larger than that for parallel pairs, as shown in Fig. 1(c). This area  $A_{exc}$  is approximated as a function of the angle  $\theta_{pp}$  between the major axes of the two proteins: [28]  $A_{exc} = a_p[4 - b_{exc}(\cos^2(\theta_{pp}) - 1)]$ . The effective excluded area is  $A_{eff} = \lambda A_{exc}$ . Although  $\lambda$  decreases slightly with an increase in the protein density, we use a constant value  $\lambda = 1/3$  for simplicity [26–28].

The bending energy of a bound protein is given as follows:

$$U_p = \frac{\kappa_p a_p}{2} (C_{\ell 1} - C_p)^2 + \frac{\kappa_{side} a_p}{2} (C_{\ell 2} - C_{side})^2, \quad (8)$$

$$C_{\ell 1} = C_1 \cos^2(\theta_{pc}) + C_2 \sin^2(\theta_{pc}), \quad (9)$$

$$C_{\ell 2} = C_1 \sin^2(\theta_{pc}) + C_2 \cos^2(\theta_{pc}), \quad (10)$$

where  $C_{\ell 1}$  and  $C_{\ell 2}$  represent the curvatures along the major and minor axes of the protein, respectively, and  $\theta_{pc}$  represents the angle between the major protein axis and membrane principal direction (the azimuthal direction of the cylindrical tube), as shown in Fig. 1(a). The proteins can have different values of bending rigidity and spontaneous curvature along the major and minor protein axes:  $\kappa_p$  and  $C_p$  along the major protein axis and  $\kappa_{side}$  and  $C_{side}$  are along the minor axis (side direction).

The free energy  $F_p$  of the bound proteins is expressed as follows:

$$F_p = \int f_p \, dA, \quad (11)$$

$$f_p = \frac{\phi k_B T}{a_p} \left[ \ln(\phi) + \frac{S\Psi}{2} - \ln \left( \int_{-\pi}^{\pi} w(\theta_{ps}) \, d\theta_{ps} \right) \right] \chi \quad (12)$$

$$w(\theta_{ps}) = g \exp \left[ \Psi s_p(\theta_{ps}) + \bar{\Psi} \sin(\theta_{ps}) \cos(\theta_{ps}) - \frac{U_p}{k_B T} \right] \Theta(g), \quad (13)$$

$$g = 1 - \phi(b_0 - b_2 S s_p(\theta_{ps})), \quad (14)$$

where  $\Theta(x)$  denotes the unit step function and  $s_p(\theta_{ps}) = \cos^2(\theta_{ps}) - 1/2$ . The proteins are ordered as  $S = 2\langle s_p(\theta_{ps}) \rangle$ , where  $\theta_{ps}$  represents the angle between the major protein axis and the ordered direction and  $\langle \dots \rangle$  denotes the ensemble average (see Fig. 1). Factor  $g$  expresses the effect of the orientation-dependent excluded volume, where  $b_0 = (4 + b_{exc}/2)\lambda$  and  $b_2 = b_{exc}\lambda$ . At  $d_{el} = 2, 3, 4$ , and  $6$ ,  $b_{exc} = 0.840, 1.98, 3.44$ , and  $6.14$ , respectively. Non-overlapped states exist at  $g > 0$ . The ensemble average of a protein quantity  $\chi$  is given as

$$\langle \chi \rangle = \frac{\int_{-\pi}^{\pi} \chi w(\theta_{ps}) \, d\theta_{ps}}{\int_{-\pi}^{\pi} w(\theta_{ps}) \, d\theta_{ps}}. \quad (15)$$

The quantities  $\Psi$  and  $\bar{\Psi}$  are the symmetric and asymmetric components of the nematic tensor, respectively, and are determined using  $S$  and  $\langle \sin(\theta_{ps}) \cos(\theta_{ps}) \rangle = 0$  via eqn (15). When the nematic order is parallel to one of the directions of the membrane principal curvatures ( $\theta_{sc} = 0$  or  $\pi/2$ ),  $\bar{\Psi} = 0$ . In this study, the integral is performed in the range of  $-\pi < \theta_{ps} \leq \pi$ . Since the shape is rotationally symmetric, the range  $-\pi/2 < \theta_{ps} \leq \pi/2$  can be used alternatively, in which the chemical potential is shifted by  $\Delta\mu = k_B T \ln(2)$  [42]. Note that the separate integrals for the bending energy and other terms used in Ref. 43 are not applicable, since the orientational fluctuations of proteins are significantly large [26, 28].

Since an external force  $f_{ex}$  is imposed, the free energy of the membrane tether is given as  $F = F_p + U_{mb} - f_{ex} L_{cy}$ , where the energy of the bare (unbound) membrane is  $U_{mb} = \kappa_d A / 2R_{cy}^2$ . This force  $f_{ex}$  is balanced with the membrane axial force and is obtained using  $\partial F / \partial L_{cy}|_{\phi} = 0$ , as follows:

$$f_{ex} = 2\pi \frac{\partial f_p}{\partial(1/R_{cy})} \Big|_{\phi} + f_{mb}. \quad (16)$$

Here, the last term  $f_{\text{mb}}$  represents the force of the bare membrane tube:  $f_{\text{mb}} = 2\pi\kappa_d/R_{\text{cy}}$ .

The equilibrium of binding and unbinding is obtained by minimizing  $F - \mu N_p$ , where  $\mu$  represents the binding chemical potential. Thus, the protein density is balanced at  $\mu = a_p \partial f_p / \partial \phi$ . Details are described in Refs. 26 and 28.

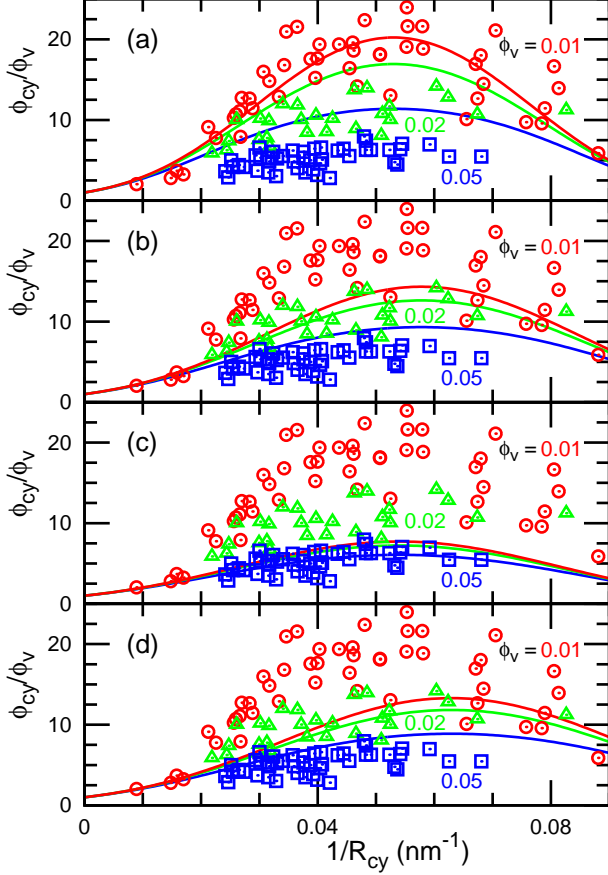


FIG. 2. Fitting of the density-curvature curves for I-BAR-domain binding based on the isotropic protein model. The density  $\phi_{\text{cy}}$  is normalized by  $\phi_v$  for the curvature  $1/R_{\text{cy}}$  of the tethered membrane. Circles, triangles, and squares indicate the experimental data for  $\phi_v = 0.01, 0.02$ , and  $0.05$ , respectively (reproduced from Ref. 14). The solid lines are given by eqn (5) with the fitting parameters  $\kappa_{\text{dif}}$  and  $C_s$ ; from top to bottom,  $\phi_v = 0.01, 0.02$ , and  $0.05$ . (a) Data at  $\phi_v = 0.01$  are fitted:  $\kappa_{\text{dif}}/k_B T = 45.9$  and  $C_s = 0.0530 \text{ nm}^{-1}$ . (b) Data at  $\phi_v = 0.02$  are fitted:  $\kappa_{\text{dif}}/k_B T = 33.6$  and  $C_s = 0.0578 \text{ nm}^{-1}$ . (c) Data at  $\phi_v = 0.05$  are fitted:  $\kappa_{\text{dif}}/k_B T = 29.0$  and  $C_s = 0.0540 \text{ nm}^{-1}$ . (d) All data are fitted:  $\kappa_{\text{dif}}/k_B T = 27.5$  and  $C_s = 0.0629 \text{ nm}^{-1}$ .

Since we consider a low density of bound proteins, the proteins in the spherical vesicle region are randomly oriented, that is,  $S = \Psi = \bar{\Psi} = 0$ . Hence, the free energy density  $f_{p,v}$  of the spherical vesicle region is given as

$$f_{p,v} = \frac{\phi_v}{a_p} \left\{ k_B T [\ln(\phi_v) - \ln(1 - b_0 \phi_v) - \ln(2\pi)] + U_{p,v} \right\}, \quad (17)$$

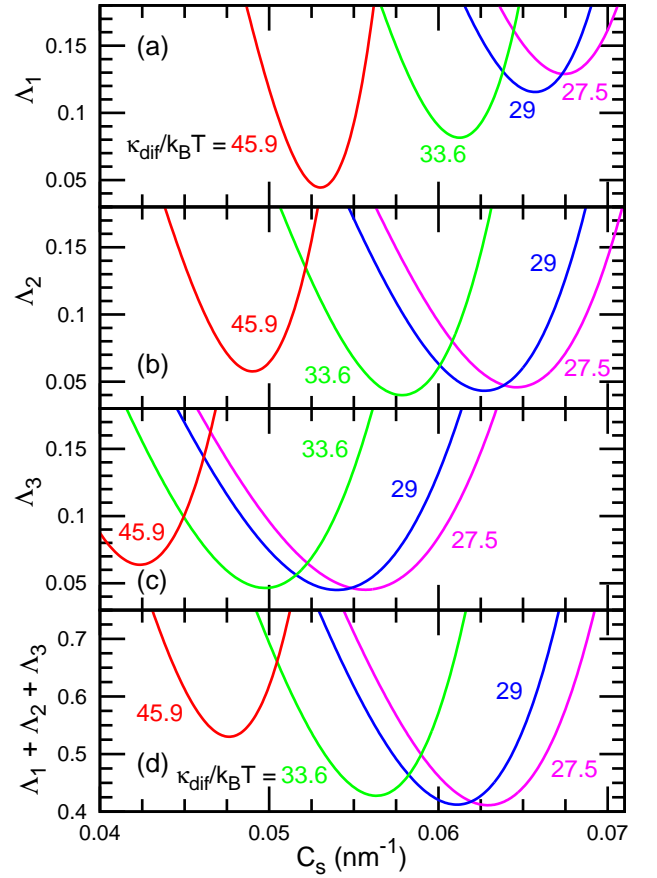


FIG. 3. Fit deviation as a function of the sensing curvature  $C_s$  for I-BAR-domain binding based on the isotropic protein model. From left to right,  $\kappa_{\text{dif}}/k_B T = 45.9, 33.6, 29$ , and  $27.5$ . (a) Fit deviation  $\Lambda_1$  for  $\phi_v = 0.01$ . The minimum  $\Lambda_1^{\text{min}} = 0.0444$  is obtained at  $\kappa_{\text{dif}}/k_B T = 45.9$  and  $C_s = 0.0530 \text{ nm}^{-1}$  (corresponding to Fig. 2(a)). (b) Fit deviation  $\Lambda_2$  for  $\phi_v = 0.02$ . The minimum  $\Lambda_2^{\text{min}} = 0.0399$  is obtained at  $\kappa_{\text{dif}}/k_B T = 33.6$  and  $C_s = 0.0578 \text{ nm}^{-1}$  (corresponding to Fig. 2(b)). (c) Fit deviation  $\Lambda_3$  for  $\phi_v = 0.05$ . The minimum  $\Lambda_3^{\text{min}} = 0.0450$  is obtained at  $\kappa_{\text{dif}}/k_B T = 29.0$  and  $C_s = 0.0540 \text{ nm}^{-1}$  (corresponding to Fig. 2(c)). (d) Sum of fit deviations  $\Lambda_1 + \Lambda_2 + \Lambda_3$ . The minimum  $(\Lambda_1 + \Lambda_2 + \Lambda_3)^{\text{min}} = 0.411$  is obtained at  $\kappa_{\text{dif}}/k_B T = 27.5$  and  $C_s = 0.0629 \text{ nm}^{-1}$  (corresponding to Fig. 2(d)).

where  $U_{p,v} = (\kappa_p C_p^2 + \kappa_{\text{side}} C_{\text{side}}^2) a_p / 2$ . Hence,  $\mu$  for the density  $\phi_v$  is obtained as

$$\frac{\mu - U_{p,v}}{k_B T} = \ln \left( \frac{\phi_v}{1 - b_0 \phi_v} \right) + \frac{b_0 \phi_v}{1 - b_0 \phi_v} - \ln(2\pi) + 1. \quad (18)$$

For the I-BAR and N-BAR domains, we use  $d_{\text{el}} = 6$ , and  $3$ , respectively. For both proteins, we use  $a_p = 50 \text{ nm}^2$  in accordance with Refs. 14 and 15.

We also calculate the orientational order  $S_z$  along the tube ( $z$ ) axis, since it is more easily measured than  $S$  in experiments. When the orientational order is along the azimuthal and axial directions ( $\theta_{\text{sc}} = 0$  and  $\pi/2$ ),  $S_z = -S$  and  $S_z = S$ , respectively. At a high protein density

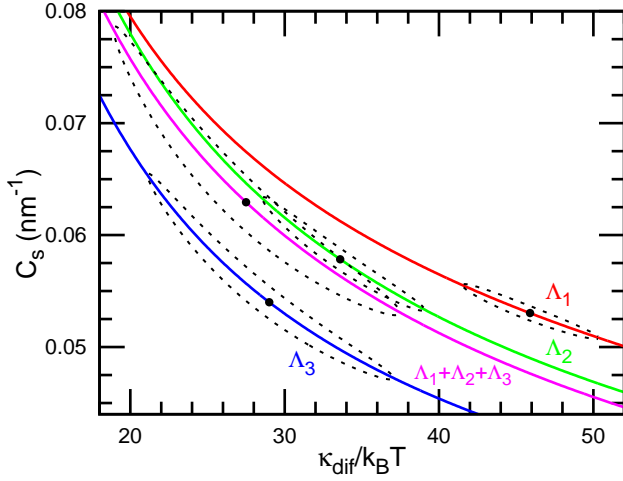


FIG. 4. Two-dimensional map of the fit deviations  $\Lambda_1$ ,  $\Lambda_2$ ,  $\Lambda_3$ , and  $\Lambda_1 + \Lambda_2 + \Lambda_3$  for I-BAR-domain binding based on the isotropic protein model. The solid lines represent the valleys connecting the values of  $C_s$  for the lowest  $\Lambda$  values at fixed  $\kappa_{\text{dif}}$ . The circles represent the minima and the dashed lines represent the contours of values exceeding the minima by 10%.

and small tube radius ( $1/R_{\text{cy}} > C_p$ ), the orientational order can deviate from the azimuthal or axial direction ( $0 < \theta_{\text{sc}} < \pi/2$ ). However, in this study, the fitted results remain in the range of  $\theta_{\text{sc}} = 0$  and  $\pi/2$ , since the protein densities are sufficiently low.

### C. Fitting

The experimental data of the bound protein density on the membrane tether are used for the fitting. We employ a least-squares method and search the conditions for minimizing the mean squared deviation:

$$\Lambda = \frac{1}{\phi_m^2 N} \sum_i^N (\phi_i - \phi_{\text{theory}})^2, \quad (19)$$

where  $N$  represents the number of experimental data, and  $\phi_i$  and  $\phi_{\text{theory}}$  represent the experimental and theoretical values of the protein density of the tether region, respectively. This fit deviation is normalized by the mean value  $\phi_m = (1/N) \sum_i \phi_i$  of the experimental data. If no normalization is applied, the obtained values of  $\Lambda$  depend on the choice of units ( $\phi_{\text{cy}}$  or  $\phi_{\text{cy}}/\phi_v$ ). For the isotropic protein model, two fitting parameters,  $\kappa_{\text{dif}}$  and  $C_0$ , are used. For the anisotropic protein model, two fitting parameters,  $\kappa_p$  and  $C_p$ , or four fitting parameters,  $\kappa_p$ ,  $C_p$ ,  $\kappa_{\text{side}}$ , and  $C_{\text{side}}$ , are used.

For the I-BAR domain of IRSp53, the experimental data reported in Ref. 14 are used. The fit deviations for  $\phi_v = 0.01$ , 0.02, and 0.05 are represented by  $\Lambda_1$ ,  $\Lambda_2$ , and  $\Lambda_3$ , respectively.

For the N-BAR domain of amphiphysin 1, the experimental data from Ref. 15 are used. We assume that

the average densities for  $n_v < 50 \mu\text{m}^{-2}$ ,  $50 \mu\text{m}^{-2} < n_v < 120 \mu\text{m}^{-2}$ , and  $120 \mu\text{m}^{-2} < n_v < 500 \mu\text{m}^{-2}$  are  $\phi_v = 0.0013$ , 0.0043, and 0.016, respectively, where  $n_v$  represents the number density of proteins in the spherical vesicle region ( $\phi_v = n_v a_p$ ). The fit deviations for  $\phi_v = 0.0013$  and 0.0043 are represented by  $\Lambda_1$  and  $\Lambda_2$ , respectively. The data of higher densities, i.e.,  $120 \mu\text{m}^{-2} < n_v < 500 \mu\text{m}^{-2}$ , are not used for the fitting, because they are widely distributed from  $\phi_{\text{cy}}/\phi_v \simeq 3$  to 20 for a narrow range of the tether curvature ( $0.04 \text{ nm}^{-1} \lesssim 1/R_{\text{cy}} \lesssim 0.11 \text{ nm}^{-1}$ ). We compare only the mean value; when the density ratio at  $1/R_{\text{cy}} = 0.07 \text{ nm}^{-1}$  is in the range  $10 \lesssim \phi_{\text{cy}}/\phi_v \lesssim 15$ , we consider the fit to be good for  $\phi_v = 0.016$ .

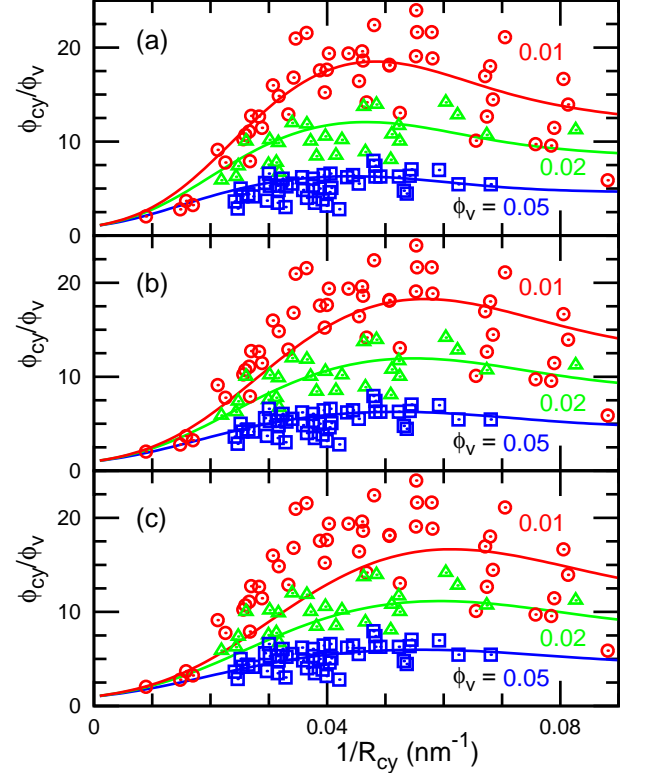


FIG. 5. Fitting of the density-curvature curves for I-BAR-domain binding based on the anisotropic protein model. Circles, triangles, and squares indicate the experimental data of  $\phi_{\text{cy}}/\phi_v$  for  $\phi_v = 0.01$ , 0.02, and 0.05, respectively (reproduced from Ref. 14). The solid lines are given by the theoretical results with the fitting parameters  $\kappa_p$  and  $C_p$  at  $\kappa_{\text{side}} = 0$ ; from top to bottom,  $\phi_v = 0.01$ , 0.02, and 0.05. (a) Data at  $\phi_v = 0.01$  are fitted:  $\kappa_p/k_B T = 100$  and  $C_p = 0.043 \text{ nm}^{-1}$ . (b) Data at  $\phi_v = 0.02$  are fitted:  $\kappa_p/k_B T = 72$  and  $C_p = 0.0505 \text{ nm}^{-1}$ . (c) Data at  $\phi_v = 0.05$  are fitted:  $\kappa_p/k_B T = 60$  and  $C_p = 0.054 \text{ nm}^{-1}$ .

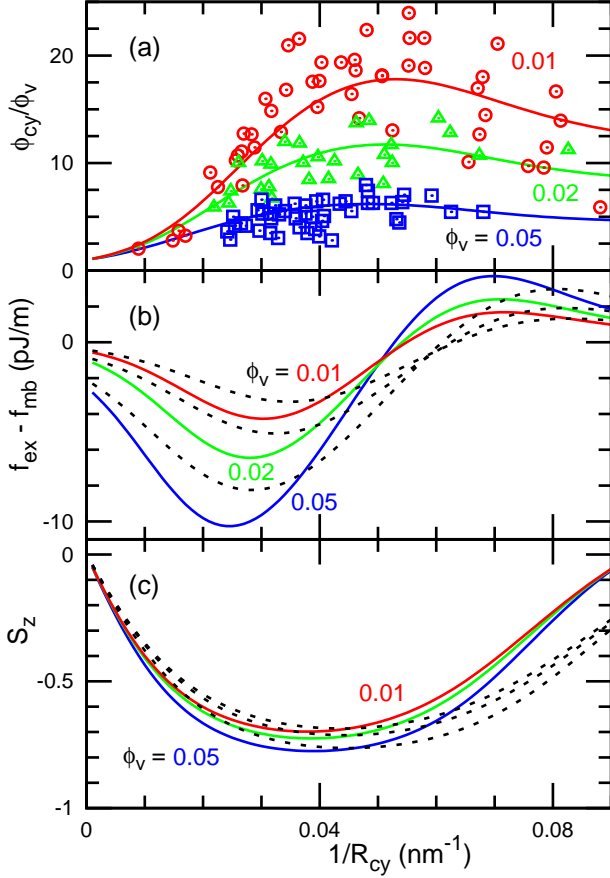


FIG. 6. Fitting of the density-curvature curves for I-BAR-domain binding based on the anisotropic protein model. The solid lines are given by the theoretical results at  $\kappa_p/k_B T = 82$  and  $C_p = 0.047 \text{ nm}^{-1}$  to minimize  $\Lambda_1 + \Lambda_2 + \Lambda_3$ . (a) Circles, triangles, and squares indicate the experimental data of  $\phi_{cy}/\phi_v$  for  $\phi_v = 0.01, 0.02$ , and  $0.05$ , respectively (reproduced from Ref. 14). (b) Force generated by the protein binding. (c) Degree  $S_z$  of protein order along the membrane tube ( $z$ ) axis. (a, c) From top to bottom,  $\phi_v = 0.01, 0.02$ , and  $0.05$ . (b) From top to bottom,  $\phi_v = 0.01, 0.02$ , and  $0.05$  at  $1/R_{cy} < 0.05 \text{ nm}^{-1}$ . The dashed lines in (b) and (c) represent the data for  $\kappa_p/k_B T = 60$  and  $C_p = 0.054 \text{ nm}^{-1}$  (the minimum value of  $\Lambda_3$  corresponding to Fig. 5(c)).

### III. BINDING OF I-BAR DOMAINS

#### A. Isotropic protein model

Before examining the anisotropic protein model, we fit the experimental data of I-BAR domains using the isotropic protein model with eqn (5). The rigidity difference  $\kappa_{dif}$  and sensing curvature  $C_s$  are fitted. Figure 2(a), (b), and (c) show the best fits for  $\phi_v = 0.01, 0.02$ , and  $0.05$ , to minimize  $\Lambda_1, \Lambda_2$ , and  $\Lambda_3$ , respectively (see Figs. 4 and 3). The target density data are fitted very well but the other two datasets exhibit large deviations. When the sum  $\Lambda_1 + \Lambda_2 + \Lambda_3$  is minimized, the obtained curves are close to the results of the fit to the middle data, i.e.,

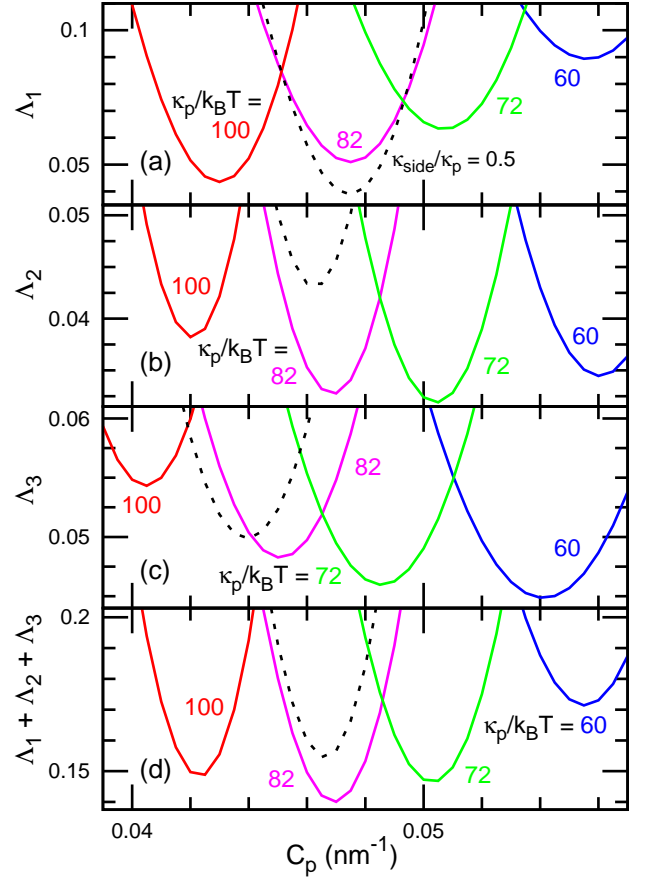


FIG. 7. Fit deviation as a function of the protein curvature  $C_p$  for I-BAR-domain binding based on the anisotropic protein model. The solid lines represent the theoretical results for  $\kappa_p/k_B T = 100, 82, 72$ , and  $60$  at  $\kappa_{side} = 0$ , from left to right. The dashed lines represent the data for  $\kappa_p/k_B T = 86$ ,  $\kappa_{side}/\kappa_p = 0.5$ , and  $C_{side} = 0$ . (a) Fit deviation  $\Lambda_1$  for  $\phi_v = 0.01$ . For  $\kappa_{side} = 0$ , the minimum value of  $\Lambda_1^{\min} = 0.044$  is obtained at  $\kappa_p/k_B T = 100$  and  $C_p = 0.043 \text{ nm}^{-1}$  (corresponding to Fig. 5(a)). For  $\kappa_{side} \neq 0$ , a lower minimum  $\Lambda_1^{\min} = 0.039$  is obtained at  $\kappa_p/k_B T = 86$ ,  $C_p = 0.0475 \text{ nm}^{-1}$ , and  $\kappa_{side}/\kappa_p = 0.5$  (corresponding to Fig. 9). (b) Fit deviation  $\Lambda_2$  for  $\phi_v = 0.02$ . The minimum  $\Lambda_2^{\min} = 0.032$  is obtained at  $\kappa_p/k_B T = 72$ ,  $C_p = 0.0505 \text{ nm}^{-1}$ , and  $\kappa_{side} = 0$  (corresponding to Fig. 5(b)). (c) Fit deviation  $\Lambda_3$  for  $\phi_v = 0.05$ . The minimum  $\Lambda_3^{\min} = 0.045$  is obtained at  $\kappa_p/k_B T = 60$ ,  $C_p = 0.054 \text{ nm}^{-1}$ , and  $\kappa_{side} = 0$  (corresponding to Fig. 5(c)). (d) Sum of fit deviations  $\Lambda_1 + \Lambda_2 + \Lambda_3$ . The minimum value  $(\Lambda_1 + \Lambda_2 + \Lambda_3)^{\min} = 0.140$  is obtained at  $\kappa_p/k_B T = 82$ ,  $C_p = 0.047 \text{ nm}^{-1}$ , and  $\kappa_{side} = 0$  (corresponding to Fig. 6).

$\Lambda_2$  (compare Fig. 2(d) and (b)). Therefore, not all of the data can be reproduced together using the isotropic protein model. Note that each dataset was fit separately (i.e., different values of the fitting parameters) in Ref. 14.

As  $\kappa_{dif}$  increases, the lowest value of  $\Lambda$  is obtained at lower  $C_s$  (see Fig. 3). This is because  $\kappa_{dif} C_s (= \kappa_{pi} C_0)$  is a factor of the major term in the exponent of eqn (5). Thus,  $\Lambda$  values close to the minimum are obtained in the long narrow regions along the solid curves in Fig. 4.



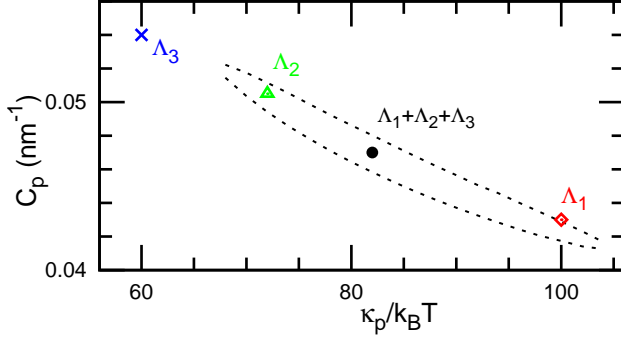


FIG. 8. Two-dimensional map of the fit deviations of  $\Lambda_1 + \Lambda_2 + \Lambda_3$  for I-BAR-domain binding based on the anisotropic protein model. The circle represents the minimum point, and the dashed lines represent the contour of values exceeding the minimum by 10%. The diamond, triangle, and cross indicate the minimum points for  $\Lambda_1$ ,  $\Lambda_2$ , and  $\Lambda_3$ , respectively.

When a statistical error is considered to be 10% of  $\Lambda$ ,  $\kappa_{\text{dif}}$  and  $C_s$  are in the regions of the long ellipses in Fig. 4. The anisotropic model exhibits a similar dependence for  $\kappa_p$  and  $C_p$  as described later.

Equation (7) for  $\phi_{\text{cy}} \ll 1$  has been used instead of eqn (5) in the previous studies [14–16, 18]. We compared the results of these two equations for  $\Lambda_1$ ,  $\Lambda_2$ , and  $\Lambda_3$  using the best-fit parameters at  $\phi_v = 0.01$ , 0.02, and 0.05, respectively. We found that the low-density limit approximation overestimates the values of  $\phi_{\text{cy}}$  by approximately 20%, 30%, and 40%, respectively. A bound protein prevents the binding of other proteins to the same position (the binding rate is proportional to  $(1 - \phi)$ ) [44]. Although this effect is negligible in the limit  $\phi_{\text{cy}} \ll 1$ , it becomes recognizable at  $\phi_{\text{cy}} \simeq 0.1$  (compare functions  $\exp(-x)$  and  $1/[1 + \exp(x)]$ ). Therefore, eqn (5) should be used in  $\phi_{\text{cy}} \gtrsim 0.1$ .

### B. Anisotropic protein model

The experimental data of the I-BAR domains are fitted using the anisotropic protein model. First, we use the protein rigidity  $\kappa_p$  and protein curvature  $C_p$  as the fitting parameters with  $\kappa_{\text{side}} = 0$ , as shown in Figs. 5–8. To determine the minimum for each fit, the parameters are varied discretely with  $\Delta\kappa_p = 2k_B T$  and  $\Delta C_p = 0.0005 \text{ nm}^{-1}$ . Very good agreement is obtained for not only the target density–curvature curve but also the other two curves (see Fig. 5). The minimum  $\Lambda$  values for the target curves are almost identical to those of the isotropic protein model (compare Fig. 7(a)–(c) and Fig. 3(a)–(c)). However, the sum,  $\Lambda_1 + \Lambda_2 + \Lambda_3$ , is significantly reduced; thus, the total fitness is improved (compare Fig. 7(d) and Fig. 3(d)).

Although the density–curvature curves are sufficiently reproduced using  $\kappa_{\text{side}} = 0$ , a deviation is recognized in  $1/R_{\text{cy}} \gtrsim 0.07 \text{ nm}^{-1}$  for  $\phi_v = 0.01$ . In the experi-

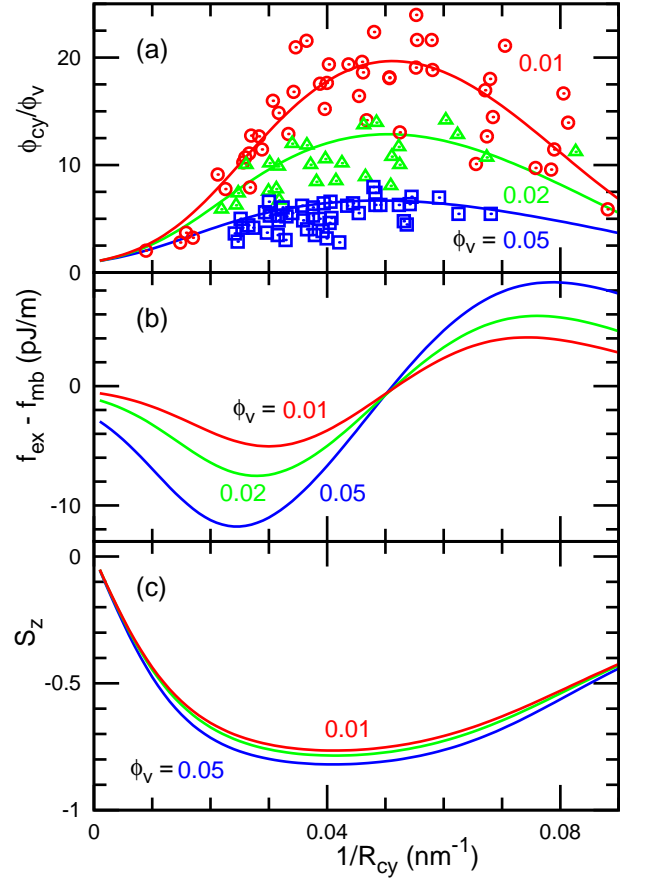


FIG. 9. Fitting of the density–curvature curves for I-BAR-domain binding based on the anisotropic protein model. The solid lines are given by the theoretical results at  $\kappa_p/k_B T = 86$ ,  $C_p = 0.0475 \text{ nm}^{-1}$ ,  $\kappa_{\text{side}}/\kappa_p = 0.5$ , and  $C_{\text{side}} = 0$  to minimize  $\Lambda_1$ . (a) Circles, triangles, and squares indicate the experimental data of  $\phi_{\text{cy}}/\phi_v$  for  $\phi_v = 0.01$ , 0.02, and 0.05, respectively (reproduced from Ref. 14). (b) Force generated by the protein binding. (c) Degree  $S_z$  of protein order along the membrane tube ( $z$ ) axis. (a, c) From top to bottom,  $\phi_v = 0.01$ , 0.02, and 0.05. (b) From top to bottom,  $\phi_v = 0.01$ , 0.02, and 0.05 at  $1/R_{\text{cy}} < 0.05 \text{ nm}^{-1}$ .

mental data, the protein density decreases by a larger amount as  $1/R_{\text{cy}}$  increases. The other two curves do not exhibit such a deviation, possibly owing to limited data for the narrow tubes (one and no data points for  $1/R_{\text{cy}} > 0.07 \text{ nm}^{-1}$  at  $\phi_v = 0.02$  and 0.05, respectively). This deviation can be eliminated by using a finite value of the bending rigidity  $\kappa_{\text{side}}$  in the side direction. In addition,  $\kappa_{\text{side}}$  is varied discretely with  $\Delta\kappa_{\text{side}} = 0.5\kappa_p$  at  $C_{\text{side}} = 0$  for  $0 \leq \kappa_{\text{side}} \leq \kappa_p$ . A better fit is obtained for  $\phi_v = 0.01$ , as shown in Figs. 7(a) and 9. Although  $C_{\text{side}}$  does not vary together here,  $\Lambda_1$  has a minimum at  $C_{\text{side}} = 0$  for the variation in  $C_{\text{side}}$  with  $\Delta C_{\text{side}} = 0.0025 \text{ nm}^{-1}$  when the other parameters are fixed. Thus, the zero side curvature is reasonable. In contrast to  $\Lambda_1$ , lower values of the others ( $\Lambda_2$ ,  $\Lambda_3$ , and  $\Lambda_1 + \Lambda_2 + \Lambda_3$ ) are not obtained using  $\kappa_{\text{side}} \neq 0$ . Thus,

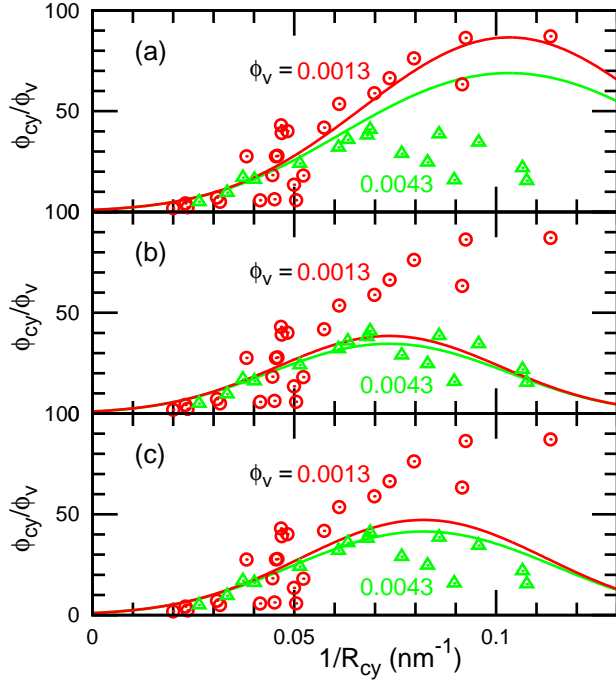


FIG. 10. Fitting of the density-curvature curves for N-BAR-domain binding based on the isotropic protein model. Circles and triangles indicate the experimental data of  $\phi_{cy}/\phi_v$  for  $\phi_v = 0.0013$  and  $0.0043$ , respectively (reproduced from Ref. 15 with permission from the Royal Society of Chemistry). The solid lines are given by eqn (5) with the fitting parameters  $\kappa_{dif}$  and  $C_s$ ; from top to bottom,  $\phi_v = 0.0013$  and  $0.0043$ . (a) Data at  $\phi_v = 0.0013$  are fitted:  $\kappa_{dif}/k_B T = 17.2$  and  $C_s = 0.1032 \text{ nm}^{-1}$ . (b) Data at  $\phi_v = 0.0043$  are fitted:  $\kappa_{dif}/k_B T = 27.4$  and  $C_s = 0.0735 \text{ nm}^{-1}$ . (c) Both datasets are fitted:  $\kappa_{dif}/k_B T = 23.3$  and  $C_s = 0.0820 \text{ nm}^{-1}$ .

the best fit for the total data ( $(\Lambda_1 + \Lambda_2 + \Lambda_3)^{\min} = 0.140$ ) is given at  $\kappa_{side} = 0$ , as shown in Fig. 6.

When a 10% larger value of  $\Lambda_1 + \Lambda_2 + \Lambda_3$  is allowed as a statistical error, the elliptical region surrounded by dashed lines in Fig. 8 is the expected range of  $\kappa_p$  and  $C_p$ . The minimum points of  $\Lambda_1$  and  $\Lambda_2$  are also included in this range. Hence, we concluded that the I-BAR domain has  $\kappa_p/k_B T = 82 \pm 20$  and  $C_p(\text{nm}^{-1}) = 0.047 - 0.0003(\kappa_p/k_B T - 82) \pm 0.001$ .

Although the experimental data are well-fitted without the side rigidity, the existence of the side rigidity is not excluded. The measurement of other quantities can increase the estimation accuracy for the mechanical properties of proteins. Here, we propose the force  $f_{ex}$  and orientational degree  $S_z$  along the tube axis as candidates. The force  $f_{ex}$  has been experimentally measured from the position of optically trapped beads [45, 46]. Force modification due to the binding of BAR domains has been reported [13, 14]. Although  $S_z$  has not been experimentally measured, it is measurable using polarizers in principle. As the tube curvature  $1/R_{cy}$  increases, the two quantities vary in different manners with respect to the protein density, as shown in Figs. 6 and 9. Each has a mini-

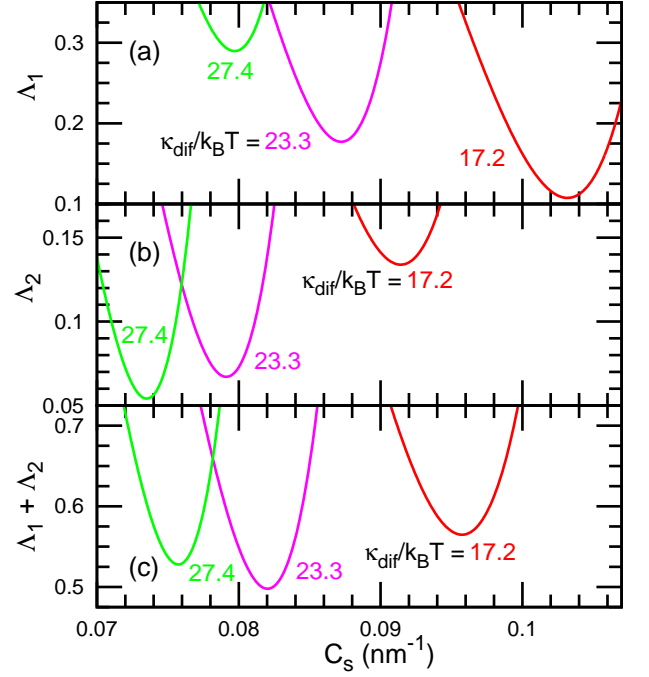


FIG. 11. Fit deviation as a function of the sensing curvature  $C_s$  for N-BAR-domain binding based on the isotropic protein model. From left to right,  $\kappa_{dif}/k_B T = 27.4$ ,  $23.3$ , and  $17.2$ . (a) Fit deviation  $\Lambda_1$  for  $\phi_v = 0.0013$ . The minimum  $\Lambda_1^{\min} = 0.1075$  is obtained at  $\kappa_{dif}/k_B T = 17.2$  and  $C_s = 0.1032 \text{ nm}^{-1}$  (corresponding to Fig. 10(a)). (b) Fit deviation  $\Lambda_2$  for  $\phi_v = 0.0043$ . The minimum  $\Lambda_2^{\min} = 0.0541$  is obtained at  $\kappa_{dif}/k_B T = 27.4$  and  $C_s = 0.0735 \text{ nm}^{-1}$  (corresponding to Fig. 10(b)). (c) Sum of fit deviations  $\Lambda_1 + \Lambda_2$ . The minimum  $(\Lambda_1 + \Lambda_2)^{\min} = 0.498$  is obtained at  $\kappa_{dif}/k_B T = 23.3$  and  $C_s = 0.0820 \text{ nm}^{-1}$  (corresponding to Fig. 10(c)).

um value at a tube curvature lower than the sensing curvature. Since the densities are sufficiently low,  $S_z$  exhibits only a small dependence on  $\phi_v$ . Importantly, they vary with changes in the bending parameters, although the density curves do not vary significantly (compare the solid and dashed lines in Fig. 6(b) and (c), and also see Fig. 9(b) and (c)). This suggests that the bending rigidity and curvature of proteins can be more accurately estimated through additional fitting of  $f_{ex}$  and  $S_z$  to the experimental data.

## IV. BINDING OF N-BAR DOMAINS

### A. Isotropic protein model

In this section, we consider the binding of N-BAR domains reported in Refs. 13 and 15. First, we examine the isotropic protein model, as for the I-BAR domains considered in Sec. III. Figures 10 and 11 show the fitted density-curvature curves and fit deviations, respectively, using eqn (5). The target curve is well-fitted, whereas the other is not, similar to the case of the I-BAR domain.



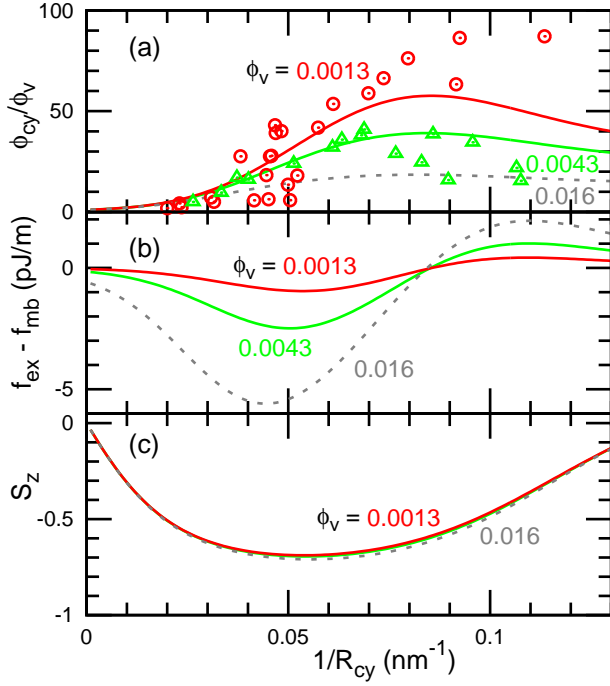


FIG. 12. Fitting of the density-curvature curves for N-BAR-domain binding based on the anisotropic protein model. The lines are given by the theoretical results at  $\kappa_p/k_B T = 39$ ,  $C_p = 0.072 \text{ nm}^{-1}$ , and  $\kappa_{\text{side}} = 0$  for minimizing  $\Lambda_1 + \Lambda_2$ . (a) Circles and triangles indicate the experimental data of  $\phi_{\text{cy}}/\phi_v$  for  $\phi_v = 0.0013$  and  $0.0043$ , respectively (reproduced from Ref. 15 with permission from the Royal Society of Chemistry). (b) Force generated by the protein binding. (c) Degree  $S_z$  of protein order along the membrane tube ( $z$ ) axis. (a, c) From top to bottom,  $\phi_v = 0.0013$ ,  $0.0043$ , and  $0.016$ . (b) From top to bottom,  $\phi_v = 0.0013$ ,  $0.0043$ , and  $0.016$  at  $1/R_{\text{cy}} < 0.08 \text{ nm}^{-1}$ .

### B. Anisotropic protein model

The experimental data of the N-BAR domains are fitted using the anisotropic protein model. First, the fitting is performed using the fitting parameters  $\kappa_p$  and  $C_p$  at  $\kappa_{\text{side}} = 0$ . The parameters are varied discretely with  $\Delta\kappa_p = k_B T$  and  $\Delta C_p = 0.0005 \text{ nm}^{-1}$ . Figure 12(a) shows the fitted density-curvature curves for minimizing  $\Lambda_1 + \Lambda_2$ . The two curves exhibit far better agreements than those obtained using the isotropic protein model (compare Figs. 12(a) and 10(c)). Nonetheless, the deviations from the curves fitted to the data for  $\phi_v = 0.0013$  or  $0.0043$  are large. Additionally, the curve obtained for  $\phi_v = 0.016$  is slightly exceeded the expected values ( $\phi_{\text{cy}}/\phi_v = 18$  at  $1/R_{\text{cy}} = 0.07 \text{ nm}^{-1}$ , as indicated by the dashed line in Fig. 12(a)).

The fit deviation of the curve minimizing  $\Lambda_1$  is identical to that of the isotropic model, but that for  $\Lambda_2$  is slightly worse (see Figs. 13(a), (b) and 14). Similar to the case of the I-BAR domain with  $\phi_v = 0.01$ , this is due to the smaller reduction in  $\phi_{\text{cy}}/\phi_v$  at high tube curvatures (see Fig. 13(b)). Thus, we perform the fit with a finite side

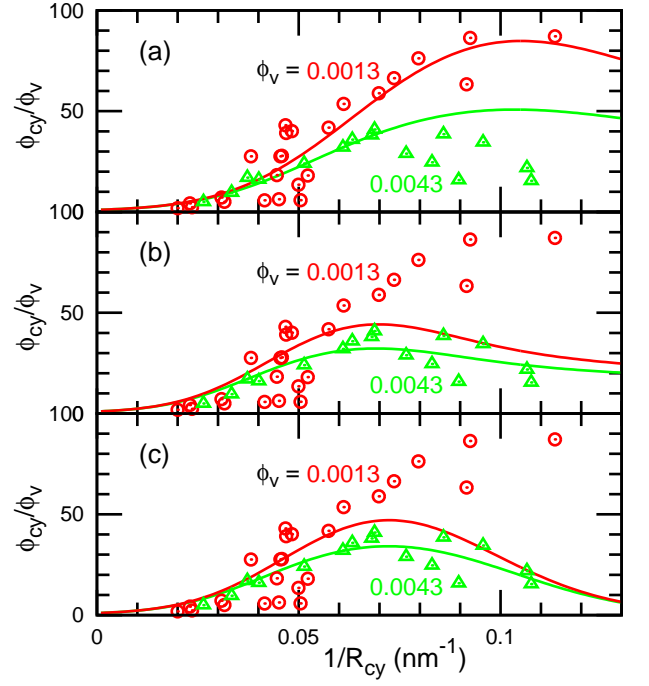


FIG. 13. Fitting of the density-curvature curves for N-BAR-domain binding based on the anisotropic protein model. Circles and triangles indicate the experimental data of  $\phi_{\text{cy}}/\phi_v$  for  $\phi_v = 0.0013$  and  $0.0043$ , respectively (reproduced from Ref. 15 with permission from the Royal Society of Chemistry). The solid lines are given by the theoretical results; from top to bottom,  $\phi_v = 0.0013$  and  $0.0043$ . (a) Data at  $\phi_v = 0.0013$  are fitted:  $\kappa_p/k_B T = 28$  and  $C_p = 0.0895 \text{ nm}^{-1}$  at  $\kappa_{\text{side}} = 0$ . (b) Data at  $\phi_v = 0.0043$  are fitted:  $\kappa_p/k_B T = 55$  and  $C_p = 0.0585 \text{ nm}^{-1}$  at  $\kappa_{\text{side}} = 0$ . (c) Data at  $\phi_v = 0.0043$  are fitted:  $\kappa_p/k_B T = 46$ ,  $C_p = 0.066 \text{ nm}^{-1}$ ,  $\kappa_{\text{side}} = 0.5\kappa_p$ , and  $C_{\text{side}} = -0.0025 \text{ nm}^{-1}$ .

rigidity for  $0 < \kappa_{\text{side}} \leq \kappa_p$ , as shown in Figs. 13(c) and 15. The parameters are varied discretely with  $\Delta\kappa_p = k_B T$ ,  $\Delta C_p = 0.001 \text{ nm}^{-1}$ ,  $\Delta\kappa_{\text{side}} = 0.5\kappa_p$ , and  $\Delta C_{\text{side}} = 0.0025 \text{ nm}^{-1}$ . A better fit to the data at  $\phi_v = 0.0043$  is obtained ( $\Lambda_2^{\text{min}}$  is 4% smaller than that of the isotropic model). For the other fit deviations ( $\Lambda_1 + \Lambda_2$  and  $\Lambda_1$ ), the minimum values are almost identical to those at  $\kappa_{\text{side}} = 0$ . Interestingly, in all cases, better fits are obtained at  $\kappa_{\text{side}}/\kappa_p = 0.5$  than at  $\kappa_{\text{side}}/\kappa_p = 1$ .

Since the density  $\phi_v$  has a wide distribution in the experimental data, we additionally performed the fitting at  $\phi_v = 0.001$  and  $0.0015$  to examine the effect of the choice of  $\phi_v$  values for  $n_v < 50 \mu\text{m}^{-2}$ . The minimum value of the sum  $\Lambda_1 + \Lambda_2$  decreases by 5% and increases by 4% for  $\phi_v = 0.001$  and  $0.0015$ , ( $(\Lambda_1 + \Lambda_2)^{\text{min}} = 0.336$  and  $0.368$ ), respectively. The corresponding values of  $\kappa_p/k_B T$  and  $C_p$  ( $\text{nm}^{-1}$ ) are shifted by only 1 and  $0.001$ , respectively. For  $\Lambda_1$ ,  $\kappa_p/k_B T$  and  $C_p$  ( $\text{nm}^{-1}$ ) are shifted by only 2 and  $0.0025$ , respectively, and the minimum value does not change. Therefore, a slight variation in  $\phi_v$  does not result in a significant change.

Next, we consider the effects of variations in the other

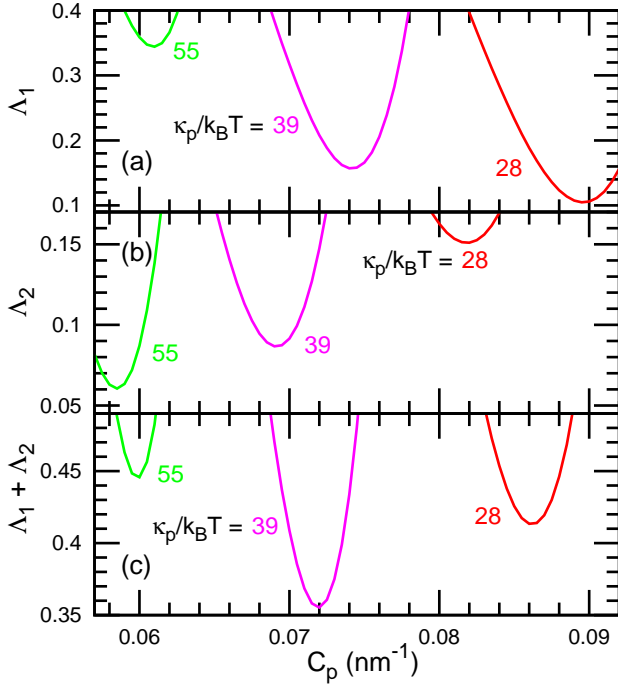


FIG. 14. Fit deviation as a function of the protein curvature  $C_p$  for N-BAR-domain binding based on the anisotropic protein model at  $\kappa_{\text{side}} = 0$ . From left to right,  $\kappa_p/k_B T = 55$ , 39, and 28. (a) Fit deviation  $\Lambda_1$  for  $\phi_v = 0.0013$ . The minimum  $\Lambda_1^{\min} = 0.105$  is obtained at  $\kappa_p/k_B T = 28$  and  $C_p = 0.0895 \text{ nm}^{-1}$  (corresponding to Fig. 13(a)). (b) Fit deviation  $\Lambda_2$  for  $\phi_v = 0.0043$ . The minimum  $\Lambda_2^{\min} = 0.061$  is obtained at  $\kappa_p/k_B T = 55$  and  $C_p = 0.0585 \text{ nm}^{-1}$  (corresponding to Fig. 13(b)). (c) Sum of fit deviations  $\Lambda_1 + \Lambda_2$ . The minimum  $(\Lambda_1 + \Lambda_2)^{\min} = 0.355$  is obtained at  $\kappa_p/k_B T = 39$  and  $C_p = 0.072 \text{ nm}^{-1}$  (corresponding to Fig. 12).

fixed parameters. An aspect ratio of  $d_{\text{el}} = 3$  is used for the N-BAR domains. Since the protein densities are low, the excluded-volume effect is weak. We examined the cases of  $d_{\text{el}} = 2$  and 4 with the best-fit conditions, and only obtained a 5% decrease in  $(\Lambda_1 + \Lambda_2)^{\min}$  at  $d_{\text{el}} = 4$ . Thus, we concluded that the N-BAR domains have  $30 \lesssim \kappa_p/k_B T \lesssim 60$  and  $0.06 \lesssim C_p(\text{nm}^{-1}) \lesssim 0.09$ .

Note that the protein shape on the membrane surface might be modified by the membrane curvature. However, as discussed above, their effects are considered small for N-BAR domains. For other proteins that exhibit large structural changes on a membrane surface as observed in deformable colloids [47], their deformations can have significant effects.

The protein area  $a_p$  can be slightly varied by area definition. In our previous studies [26–28], we used  $a_p = 60 \text{ nm}^2$ , since the protein was approximated as elliptical with  $\ell_1 = 15 \text{ nm}$  and  $\ell_2 = 5 \text{ nm}$ , and the protein area partially included bare membrane regions. To fit a density–curvature curve, the area  $a_p$  only appears as pairs with bending rigidities in the theoretical models ( $a_p \kappa_p$  and  $a_p \kappa_{\text{side}}$  in the anisotropic model and  $a_p \kappa_{\text{dif}}$  in the isotropic model). Thus, the area variation influences

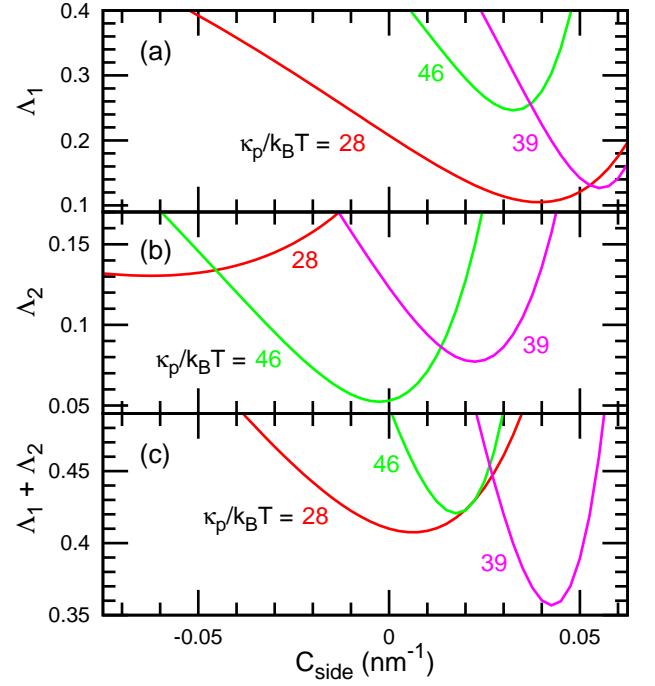


FIG. 15. Fit deviation as a function of the side curvature  $C_{\text{side}}$  for N-BAR-domain binding based on the anisotropic protein model at  $\kappa_{\text{side}} > 0$ . From left to right,  $(\kappa_p/k_B T, C_p (\text{nm}^{-1})) = (28, 0.087)$ ,  $(46, 0.066)$ , and  $(39, 0.068)$  with  $\kappa_{\text{side}}/\kappa_p = 0.5$ . (a) Fit deviation  $\Lambda_1$  for  $\phi_v = 0.0013$ . The minimum  $\Lambda_1^{\min} = 0.105$  is obtained at  $(\kappa_p/k_B T, C_p (\text{nm}^{-1}), C_{\text{side}} (\text{nm}^{-1}), \kappa_{\text{side}}/\kappa_p) = (28, 0.087, 0.04, 0.5)$ . (b) Fit deviation  $\Lambda_2$  for  $\phi_v = 0.0043$ . The minimum  $\Lambda_2^{\min} = 0.052$  is obtained at  $(\kappa_p/k_B T, C_p (\text{nm}^{-1}), C_{\text{side}} (\text{nm}^{-1}), \kappa_{\text{side}}/\kappa_p) = (46, 0.066, -0.0025, 0.5)$  (Fig. 13(c)). (c) Sum of fit deviations  $\Lambda_1 + \Lambda_2$ . The minimum  $(\Lambda_1 + \Lambda_2)^{\min} = 0.357$  is obtained at  $(\kappa_p/k_B T, C_p (\text{nm}^{-1}), C_{\text{side}} (\text{nm}^{-1}), \kappa_{\text{side}}/\kappa_p) = (39, 0.068, 0.0425, 0.5)$ .

the bending rigidity in accordance with  $\kappa' = \kappa a_p/a'_p$  (e.g., a 20% decrease in  $a_p$  results in a 25% increase in the bending rigidities). The force,  $f_{\text{ex}} - f_{\text{mb}}$ , is also modified by the factor  $a_p/a'_p$ . When the protein density is measured as the number density  $n_v$ , the area fraction is slightly modified according to the area definition ( $\phi_v = n_v a_p$ ). However, this results in only slight changes, as discussed above.

In our previous study [28], we compared the results of the anisotropic model and a coarse-grained membrane simulation. When the proteins are distributed homogeneously in the membrane, the results agree very well. In contrast, deviations are obtained, when the proteins form small clusters. Since the clusters have a larger area than the individual proteins, they are more oriented in the preferred direction. The ratio of the clusters increases with the protein density. Thus, we consider that the deviation in this study suggests non-negligible cluster formation of the N-BAR domains. Note that the clustering can be induced by direct attractive interaction between proteins and membrane-mediated interactions. Large clusters can

deform a membrane tube into polygonal shapes [38, 48].

## V. SUMMARY

We have developed an estimation method for the mechanical properties of bound proteins based on the experiments of tethered vesicles and applied it to the I-BAR and N-BAR domains. When the anisotropy of the proteins is taken into account, the experimental data are reproduced far better. When the classical isotropic model is used, each density–curvature curve is well reproduced but the other curves largely deviate. When the recently developed anisotropic model is used, this deviation is significantly reduced. For the I-BAR domains, all three curves are well-fitted by a single parameter set, and the bending rigidity  $\kappa_p/k_B T = 82$  and spontaneous curvature  $C_p(\text{nm}^{-1}) = 0.047$  along the protein axis are determined. The estimation errors are small along  $\kappa_p C_p$  as  $\delta_{\text{er}}(\kappa_p/k_B T) = \pm 20$  and  $\delta_{\text{er}}(C_p(\text{nm}^{-1})) = -0.0003(\kappa_p/k_B T - 82) \pm 0.001$ . For the N-BAR domains, the two density–curvature curves are not completely fitted simultaneously, even when the anisotropic model is used. This deviation is likely caused by a small cluster formation, and  $30 \lesssim \kappa_p/k_B T \lesssim 60$  and  $0.06 \lesssim C_p(\text{nm}^{-1}) \lesssim 0.09$  are estimated. If the definition of the protein area is modified, the bending rigidity is changed as  $\kappa'_p = \kappa_p a_p/a'_p$ .

The experimental data were well-fitted without the

side bending rigidity. Including them, the fitness was improved for some of the conditions but the others were not changed significantly. Since positive and negative side curvatures can promote and suppress the tubulation, respectively [49], the estimation of the side rigidity and side curvature is important. Recent experiments [23, 50–52] revealed that the intrinsically disordered domains of curvature-inducing proteins play a significant role in membrane remodeling. The disordered domains can be modeled by excluded-volume chains. At a low protein density, the membrane–chain interaction slightly increases the bending rigidity and spontaneous curvature isotropically (i.e., in both the axial and side directions of proteins) [53–56]. At a high density, the inter-chain interactions have strong effects in protein clusters [53, 57–59] and also between the clusters [56, 59]. These effects should be further examined by the comparison of tether-vesicle experiments.

In this study, we fitted only the density–curvature curves. The estimation quality can be further improved by additional fitting for other quantities. For this purpose, we have proposed two parameters, the axial force and the orientational degree. They exhibit different behaviors from the density–curvature curve; thus, comparison with the experimental results can facilitate the determination of the mechanical properties.

## ACKNOWLEDGMENTS

This work was supported by JSPS KAKENHI Grant Number JP21K03481.

- 
- [1] H. T. McMahon and J. L. Gallop, *Nature* **438**, 590 (2005).
  - [2] S. Suetsugu, S. Kurisu, and T. Takenawa, *Physiol. Rev.* **94**, 1219 (2014).
  - [3] L. Johannes, R. G. Parton, P. Bassereau, and S. Mayor, *Nat. Rev. Mol. Cell Biol.* **16**, 311 (2015).
  - [4] F. Brandizzi and C. Barlowe, *Nat. Rev. Mol. Cell Biol.* **14**, 382 (2013).
  - [5] J. H. Hurley, E. Boura, L.-A. Carlson, and B. Różycki, *Cell* **143**, 875 (2010).
  - [6] H. T. McMahon and E. Boucrot, *Nat. Rev. Mol. Cell Biol.* **12**, 517 (2011).
  - [7] T. Baumgart, B. R. Capraro, C. Zhu, and S. L. Das, *Annu. Rev. Phys. Chem.* **62**, 483 (2011).
  - [8] C. Has and S. L. Das, *Biochim. Biophys. Acta* **1865**, 129971 (2021).
  - [9] T. Itoh and P. De Camilli, *Biochim. Biophys. Acta* **1761**, 897 (2006).
  - [10] M. Masuda and N. Mochizuki, *Semin. Cell Dev. Biol.* **21**, 391 (2010).
  - [11] C. Mim and V. M. Unger, *Trends Biochem. Sci.* **37**, 526 (2012).
  - [12] A. Frost, R. Perera, A. Roux, K. Spasov, O. Destaing, E. H. Egelman, P. De Camilli, and V. M. Unger, *Cell* **132**, 807 (2008).
  - [13] B. Sorre, A. Callan-Jones, J. Manzi, B. Goud, J. Prost, P. Bassereau, and A. Roux, *Proc. Natl. Acad. Sci. USA* **109**, 173 (2012).
  - [14] C. Prévost, H. Zhao, J. Manzi, E. Lemichez, P. Lappalainen, A. Callan-Jones, and P. Bassereau, *Nat. Commun.* **6**, 8529 (2015).
  - [15] F.-C. Tsai, M. Simunovic, B. Sorre, A. Bertin, J. Manzi, A. Callan-Jones, and P. Bassereau, *Soft Matter* **17**, 4254 (2021).
  - [16] K. R. Rosholm, N. Leijnse, A. Mantsiou, V. Tkach, S. L. Pedersen, V. F. Wirth, L. B. Oddershede, K. J. Jensen, K. L. Martinez, N. S. Hatzakis, P. M. Bendix, A. Callan-Jones, and D. Stamou, *Nat. Chem. Biol.* **13**, 724 (2017).
  - [17] S. Aimon, A. Callan-Jones, A. Berthaud, M. Pinot, G. E. Toombes, and P. Bassereau, *Dev. Cell* **28**, 212 (2014).
  - [18] S. Yang, X. Miao, S. Arnold, B. Li, A. T. Ly, H. Wang, M. Wang, X. Guo, M. Pathak, W. Zhao, C. D. Cox, and Z. Shi, *Nat. Commun.* **13**, 7467 (2022).
  - [19] A. Roux, G. Koster, M. Lenz, B. Sorre, J.-B. Manneville, P. Nassoy, and P. Bassereau, *Proc. Natl. Acad. Sci. USA* **107**, 4141 (2010).
  - [20] G. Moreno-Pescador, C. D. Florentsen, H. Østbye, S. L. Sønder, T. L. Boye, E. L. Veje, A. K. Sonne, S. Semsey, J. Nylandsted, R. Daniels, and P. M. Bendix, *ACS Nano* **13**, 6689 (2019).
  - [21] J. B. Larsen, K. R. Rosholm, C. Kennard, S. L. Pedersen, H. K. Munch, V. Tkach, J. J. Sakon, T. Bjørnholm, K. R.

- Weninger, P. M. Bendix, K. J. Jensen, N. S. Hatzakis, M. J. Uline, and D. Stamou, ACS Cent. Sci. **6**, 1159 (2020).
- [22] N. S. Hatzakis, V. K. Bhatia, J. Larsen, K. L. Madsen, P.-Y. Bolinger, A. H. Kunding, J. Castillo, U. Gether, P. Hedegård, and D. Stamou, Nat. Chem. Biol. **5**, 835 (2009).
- [23] W. F. Zeno, W. T. Snead, A. S. Thatte, and J. C. Stachowiak, Soft Matter **15**, 8706 (2019).
- [24] P. B. Canham, J. Theor. Biol. **26**, 61 (1970).
- [25] W. Helfrich, Z. Naturforsch **28c**, 693 (1973).
- [26] C. Tozzi, N. Walani, A.-L. L. Roux, P. Roca-Cusachs, and M. Arroyo, Soft Matter **17**, 3367 (2021).
- [27] A.-L. L. Roux, C. Tozzi, N. Walani, X. Quiroga, D. Zalvidea, X. Trepas, M. Staykova, M. Arroyo, and P. Roca-Cusachs, Nat. Commun. **12**, 6550 (2021).
- [28] H. Noguchi, C. Tozzi, and M. Arroyo, Soft Matter **18**, 3384 (2022).
- [29] E. S. Nascimento, P. Palfy-Muhoray, J. M. Taylor, E. G. Virga, and X. Zheng, Phys. Rev. E **96**, 022704 (2017).
- [30] P. G. Dommersnes and J.-B. Fournier, Eur. Phys. J. B **12**, 9 (1999).
- [31] P. G. Dommersnes and J.-B. Fournier, Biophys. J. **83**, 2898 (2002).
- [32] Y. Schweitzer and M. M. Kozlov, PLoS Comput. Biol. **11**, e1004054 (2015).
- [33] T. Kohyama, J. Phys. Soc. Jpn. **88**, 024008 (2019).
- [34] H. Noguchi and J.-B. Fournier, Soft Matter **13**, 4099 (2017).
- [35] A.-S. Smith, E. Sackmann, and U. Seifert, Phys. Rev. Lett. **92**, 208101 (2004).
- [36] H. Noguchi, Soft Matter **17**, 10469 (2021).
- [37] H. Noguchi, Phys. Rev. E **104**, 014410 (2021).
- [38] H. Noguchi, Int. J. Mod. Phys. B **36**, 2230002 (2022).
- [39] S. A. Safran, *Statistical Thermodynamics of Surfaces, Interfaces, and Membranes* (Addison-Wesley, Reading, MA, 1994).
- [40] S. Ramaswamy, J. Toner, and J. Prost, Phys. Rev. Lett. **84**, 3494 (2000).
- [41] C. Tozzi, N. Walani, and M. Arroyo, New J. Phys. **21**, 093004 (2019).
- [42] In Ref. 28, the formula is written for  $-\pi/2 < \theta_{ps} \leq \pi/2$ , but the chemical potential and axial forces are inconsistently calculated.
- [43] P. Vyas, P. B. S. Kumar, and S. L. Das, Soft Matter **18**, 1653 (2022).
- [44] Q. Goutaland, F. van Wijland, J.-B. Fournier, and H. Noguchi, Soft Matter **17**, 5560 (2021).
- [45] V. Heinrich and R. E. Waugh, Ann. Biomed. Eng. **24**, 595 (1996).
- [46] R. Dimova, Adv. Colloid Interface Sci. **208**, 225 (2014).
- [47] J. Midya, T. Auth, and G. Gompper, ACS Nano **17**, 1935 (2023).
- [48] H. Noguchi, J. Chem. Phys. **143**, 243109 (2015).
- [49] H. Noguchi, Sci. Rep. **6**, 20935 (2016).
- [50] J. C. Stachowiak, E. M. Schmid, C. J. Ryan, H. S. Ann, D. Y. Sasaki, M. B. Sherman, P. L. Geissler, D. A. Fletcher, and C. C. Hayden, Nat. Cell Biol. **14**, 944 (2012).
- [51] D. J. Busch, J. R. Houser, C. C. Hayden, M. B. Sherman, E. M. Lafer, and J. C. Stachowiak, Nat. Commun. **6**, 7875 (2015).
- [52] W. T. Snead, W. F. Zeno, G. Kago, R. W. Perkins, J. B. Richter, C. Zhao, E. M. Lafer, and J. C. Stachowiak, J. Cell Biol. **218**, 664 (2019).
- [53] C. Hiergeist and R. Lipowsky, J. Phys. II France **6**, 1465 (1996).
- [54] T. Bickel, C. Jeppesen, and C. M. Marques, Eur. Phys. J. E **4**, 33 (2001).
- [55] T. Auth and G. Gompper, Phys. Rev. E **68**, 051801 (2003).
- [56] H. Wu, H. Shiba, and H. Noguchi, Soft Matter **9**, 9907 (2013).
- [57] D. Marsh, R. Bartucci, and L. Sportelli, Biochim. Biophys. Acta **1615**, 33 (2003).
- [58] A. R. Evans, M. S. Turner, and P. Sens, Phys. Rev. E **67**, 041907 (2003).
- [59] H. Noguchi, J. Chem. Phys. **157**, 034901 (2022).